UNITED TECHNOLOGIES
PRATT & WHITNEY

P.O. Box 109600
West Palm Beach, FL 33410-9600
(407) 796-2000

Government Engines & Space Propulsion

21 October 1994

Office of Naval Research
Scientific Officer
Attn: Dr. A. K. Vasudevan, Code 1222
800 N. Quincy Street
Arlington, Va 22217-5000

Contract No. N00014-91-C-0124
Item No. 0002, Sequence No. A001

Subject: Submittal of the Interim Progress Report, FR21998-24

Gentlemen:

In accordance with the applicable requirements of the contract, we herewith submit one (1) copy of the subject report.

Very truly yours,

UNITED TECHNOLOGIES CORPORATION
Pratt & Whitney

Original contains color plates: All DTIC reproductions will be in black and white

Margaret B Hall

Margaret B. Hall
Contract Data Coordinator

cc: With Enclosures

Director, Naval Research, Code 2627
DPRO
Defense Technical Information Center (2 copies)
Dr. K. Sadananda

FATIGUE IN SINGLE CRYSTAL NICKEL SUPERALLOYS

Technical Progress Report

Daniel P. DeLuca
Principal Investigator

Charles Annis
Program Manager

UNITED TECHNOLOGIES PRATT&WHITNEY
P.O. Box 109600
West Palm Beach, FL 33410-9600
(407)796-6565
Government Engines and Space Propulsion

15 October, 1994

Period of performance
16 October 1993 through 15 October 1994

Contract N00014-91-C-0124

Prepared for:
Dr. A. K. Vasudevan, Scientific Officer
Code 1222

Office of Naval Research
Department of the Navy
800 N. Quincy Street
Arlington, Va 22217-5000

I. Introduction and Program Objective

This program investigates the seemingly unusual behavior of single crystal airfoil materials. The fatigue initiation processes in single crystal (SC) materials are significantly more complicated and involved than fatigue initiation and subsequent behavior of a (single) macrocrack in conventional, isotropic, materials. To understand these differences it is helpful to review the evolution of high temperature airfoils.

Characteristics of Single Crystal Materials

Modern gas turbine flight propulsion systems employ single crystal materials for turbine airfoil applications because of their superior performance in resisting creep, oxidation, and thermal mechanical fatigue (TMF). These properties have been achieved by composition and alloying, of course, but also by appropriate crystal orientation and associated anisotropy.

Early aeroengine turbine blade and vane materials were conventionally cast, equiaxed alloys, such as IN100 and Rene'80. This changed in the late 1960s with the introduction of directionally-solidified (DS) MAR-M200+Hf airfoils. The DS process produces a <001> crystallographic orientation, which in superalloys exhibits excellent strain controlled fatigue resistance due to its low elastic modulus. The absence of transverse grain boundaries, a 60% reduction in longitudinal modulus compared with equiaxed grains, and its corresponding improved resistance to thermal fatigue and creep, permitted significant increases in allowable metal temperatures and blade stresses. Still further progress was achieved in the mid-1970s with the development of single crystal airfoils[1].

The first such material, PWA 1480, has a considerably simpler composition than preceding cast nickel blade alloys because, in the absence of grain boundaries, no grain boundary strengthening elements are required. Deleting these grain boundary strengtheners, which are also melting point depressants, increased the incipient melt temperature. This, in turn, allowed nearly complete γ' solutioning during heat treatment and thus a reduction in dendritic segregation. The absence of grain boundaries, the opportunity for full solution heat treatment, and the minimal post-heat treat dendritic segregation, result in significantly improved properties as compared with conventionally cast or directionally solidified alloys. Single crystal castings also share with DS alloys the <001> crystal orientation, along with the benefits of the resulting low modulus in the longitudinal direction.

Pratt & Whitney has developed numerous single crystal materials. Like most, PWA 1480 and PWA 1484 are γ' strengthened cast mono grain nickel superalloys based on the Ni-Cr-Al system. The bulk of the microstructure consists of approximately 60% by volume of cuboidal γ' precipitates in a g matrix. The precipitate ranges from 0.35 to 0.5 microns and is an ordered

---

[1] Gell, M., D. N. Duhl, and A. F. Giamei, 1980, "The Development of Single Crystal Superalloy Turbine Blades," *Superalloys* 1980, proceedings of the Fourth International Symposium on Superalloys, American Society for Metals, Metal Park, Ohio, pp. 205-214

Face Centered Cubic (FCC) nickel aluminide compound. The macrostructure of these materials is characterized by parallel continuous primary dendrites spanning the casting without interruption in the direction of solidification. Secondary dendrite arms (perpendicular to solidification) define the interdendritic spacing. Solidification for both primary and secondary dendrite arms proceeds in <001> type crystallographic directions. Undissolved eutectic pools and associated microporosity reside throughout the interdendritic areas. These features act as microstuctural discontinuities, and often exert a controlling influence on the fatigue initiation behavior of the alloy. Also, since the eutectics are structurally dissimilar from the surrounding matrix their fracture characteristics will differ.

Single Crystal Fatigue

The fatigue process in single crystal airfoil materials is a remarkably complex and interesting process. In cast single crystal nickel alloys, two basic fracture modes, crystallographic and non-crystallographic, are seen in combination. They occur in varying proportions depending upon temperature and stress state. Crystallographic orientation with respect to applied load also affects the proportion of each and influences the specific crystallographic planes and slip directions involved. Mixed mode fracture is observed under monotonic as well as cyclic conditions.

Single crystal turbine blades are cast such that the radial axis of the component is essentially coincident with the <001> crystallographic direction which is the direction of solidification. Crystallographic fracture is usually seen as either octahedral along multiple (111) planes or under certain circumstances as (001) cleavage along cubic planes.

Non-crystallographic fracture is also observed. Low temperatures favor crystallographic fracture. At higher temperatures, in the 427C range, small amounts of non-crystallographic propagation have the appearance of transgranular fatigue in a related fine grain equiaxed alloy. Under some conditions, this propagation changes almost immediately to the highly crystallographic mode along (111) shear planes, frequently exhibiting prominent striations emanating from the fatigue origin and continuing to failure in overstress. Under other conditions the non-crystallographic behavior can continue until tensile failure occurs. At intermediate temperatures (around 760C) non-crystallographic propagation is more pronounced and may continue until tensile overload along (111) planes occurs, or may transition to subcritical crystallographic propagation. At 982C, propagation is almost entirely non-crystallographic, similar to transgranular propagation in a polycrystal.

Damage Catalogue

This program will identify and compile descriptions of the fracture morphologies observed in SC airfoil materials under various combinations of temperature and stress associated with advanced Navy aeropropulsion systems. We will suggest fatigue mechanisms for these morphologies and catalogue them as unique damage *states*. Most testing will be accomplished under ancillary funding, and therefore be available to this effort at no cost. The work is organized into four tasks, which are described in the following paragraphs.

II. Program Organization

The program is structured into four tasks, three technical and one reporting. The individual tasks are outlined here.

Task 100 - Micromechanical Characterization

This task will define the mechanisms of damage accumulation for the various types of fracture observed in single crystal alloys. These fracture characteristics will be used to establish a series of Damage States which represent the fatigue damage process. The basis for this investigation will be detailed fractographic assessment of failed laboratory specimens generated in concurrent programs. Emphasis will be on specifically identifying the micromechanical damage mechanisms, relating them to a damage state, and determining the conditions required to transition to an alternate state.

Task 200 - Analytical Parameter Development

This task will extend current methods of fatigue and fracture mechanics analysis to account for microstructural complexities inherent in single crystal alloys. This will be accomplished through the development of flexible correlative parameters which can be used to evaluate the crack growth characteristics of a particular damage state. The proposed analyses will consider the finite element and the hybrid Surface-Integral and Finite Element (SAFE) methods to describe the micromechanics of crack propagation.

Task 300 - Probabilistic Modeling

This task will model the accumulation of fatigue damage in single crystal alloys as a Markov process. The probabilities of damage progressing between the damage states defined in Task 100 will be evaluated for input into the Markov model. The relationship between these transition probabilities and fatigue life will then be exploited to establish a model with comprehensive life predictive capabilities.

Task 400 - Reporting

Running concurrently with the analytical portions of the program, this task will inform the Navy Program Manager and Contracting Officer of the technical and fiscal status of the program through R&D status reports.

III. Technical Progress

The micromechanics of Mode II fracture in PWA 1480 and PWA 1484 were the subject of investigation during this reporting period. The conditions favoring sub critical (111) crack growth, Stage I microscopic (111) fatigue crack initiation and global (111) propagation are of particular importance to turbine blade life prediction. To serve as a reference for the

discussions provided in this summary, two previous reports of particular relevance are included as appendices A and B.

Octahedral Fatigue Crack Initiation

Octahedral initiation has been viewed as an extension of slip (Chen[1]) with no clear distinction between the processes of fatigue crack incubation and propagation. Rather, there appears to be a critical slip displacement that when reached transitions to "glide decohesion", the beginning of (111) fracture. It has been theorized that persistent slip bands evolve as initial precipitate shearing by dislocations compromise the order in the γ' superlattice, thus creating preferential avenues for further dislocation penetration.

Based on a review of PWA 1484 failed specimens, the tendency for crystallographic versus non crystallographic fatigue crack initiation appears to be inversely dependent on temperature and stress in notched LCF (Figures 1 and 2). The trend was noted in notched low cycle fatigue tests conducted with non-hipped PWA 1484 at 1100 F, 1400 F and 1600 F. This observation suggests that an activation energy, in terms of frequency, temperature and stress, can be determined to predict the conditions favoring (111) initiation. This behavior was previously reported by Leverant [2] in single crystal Mar-M-200.

Figure 1: Crystallographic fatigue crack initiation in PWA 1484 at 1100°F.

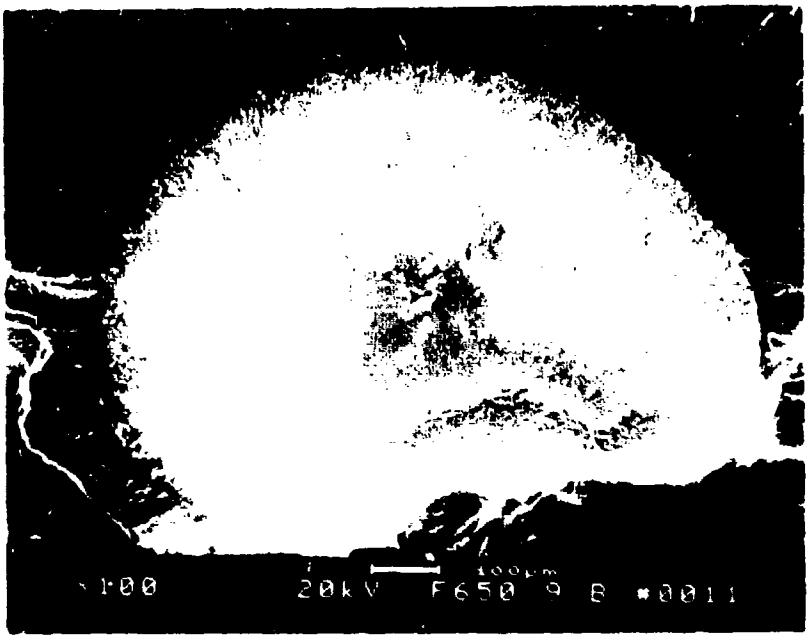

Figure 2. Non crystallographic fatigue crack initiation in PWA 1484 at 1400°F.

k_{th} and the Effects of Defects

Chen[1] confined his consideration of the actual initiation of a (111) crack to octahedral slip between (111) planes with no consideration of the effects of defects. Coherent and non coherent interfaces occur at defects such as eutectics or micro pores respectively. These species along with carbides are the principal forms of intrinsic material quality (IMQ) defects present in PWA 1480 and PWA 1484. Figures 3 and 4 show how (111) initiation is aided by the presence of IMQ defects. The alloy shown is PWA 1422, a columnar grain blade alloy used in high pressure turbine (HPT) (TF-30 / F-14A Tomcat) and low pressure turbine (LPT) applications. Although columnar grain or directionally solidified (DS) castings preclude transverse grain boundaries, they do require grain boundary strengtheners since **longitudinal** grain boundaries exist. These grain boundary strengthening elements result in an increased level of IMQ defects (carbides etc.) not only at grain boundaries but at dendrite boundaries as well. The deformation processes occurring within a grain are representative of single crystal deformation processes and the higher frequency of occurrence of IMQ species in PWA 1422 increases the chance of viewing the effect of defects on (111) fatigue crack initiation. The photograph shown in Figure 3 is of a failed compact tension fatigue crack growth specimen with the fracture plane at the top of the photograph. The nominal crack plane is parallel to (001) and the nominal load axis is ⟨001⟩. The test type was a decreasing K threshold determination followed by a constant load Region II test, both conducted at 1100 F, R 0.7,

Figure 3: Macroscopic view of Failed 1422 SEM specimen showing plastic deformation near fracture surface (32X).

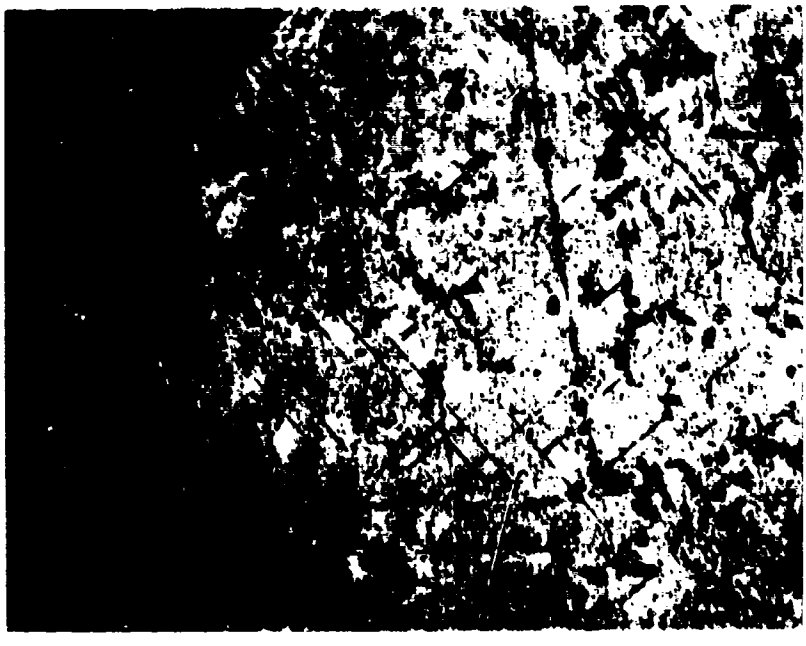

Figure 4. Enlargement of previous figure showing interdendritic defects interacting with slip bands (126X)

20 Hertz. The relatively high K_{max} values in the constant load region resulted in significant amounts of localized slip visible on the specimen sides.

A typical area of slip is shown in detail in figure 4. Interdendritic areas are delineated by microporosity, eutectic γ-γ' and carbides. Further examination reveals slip bands concentrated in these interdendritic areas. IMQ defects impede long range dislocation motion and slip bands intersecting with defects can be seen. These slip bands promote dislocation pile up at defect interfaces. In the case of a coherent particle, building stresses at defect interface eventually cleave the defect on the slip plane (Figure 5) or hasten slip band decohesion adjacent to the defect as in Figure 6. In both cases cracked portions of the slip band are evidenced by the formation of oxidation blistering along the slip line. These observations support fracture based probabilistic life prediction systems where IMQ defect distributions are sampled for initial flaw size.

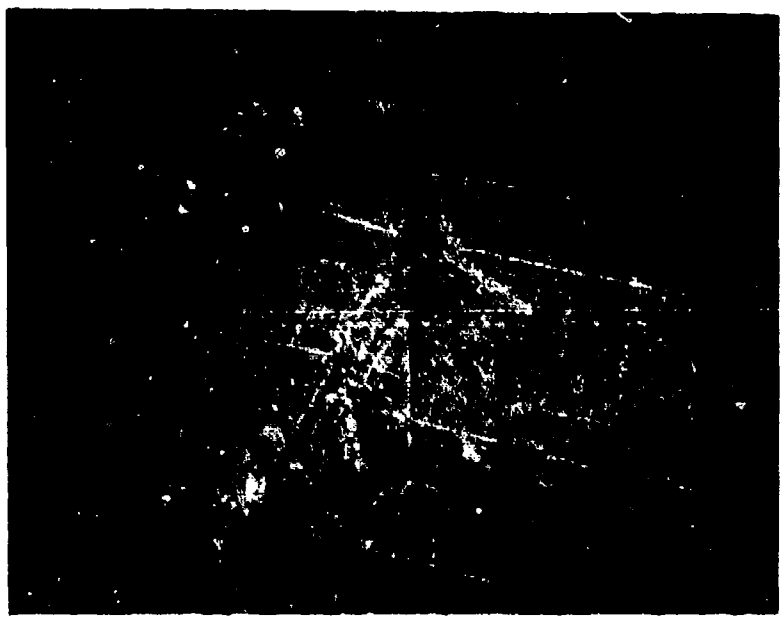

Figure 5: Slip bands cutting coherent defects (eutectic γ-γ') and slip band cracking of the defect (at oxide blisters). (500X)

Natural Small Flaw k_{th} Determination

A small (natural) flaw threshold stress intensity determination method for octahedral fatigue crack growth is of particular importance to turbine blade life prediction. An experiment was conducted to determine the natural small flaw octahedral K_{th} of PWA 1480. A vibratory (R= -1.0) go no-go approach using a short cantilever beam specimen was selected. A schematic of the specimen / strain gage nomenclature is shown in figure 7. The stress was accurately known (from strain gages). The specimen was run at resonance (1,690 Hz.)

Figure 6: Slip band intersection with micropore showing oxide blister crack initiation (315X).

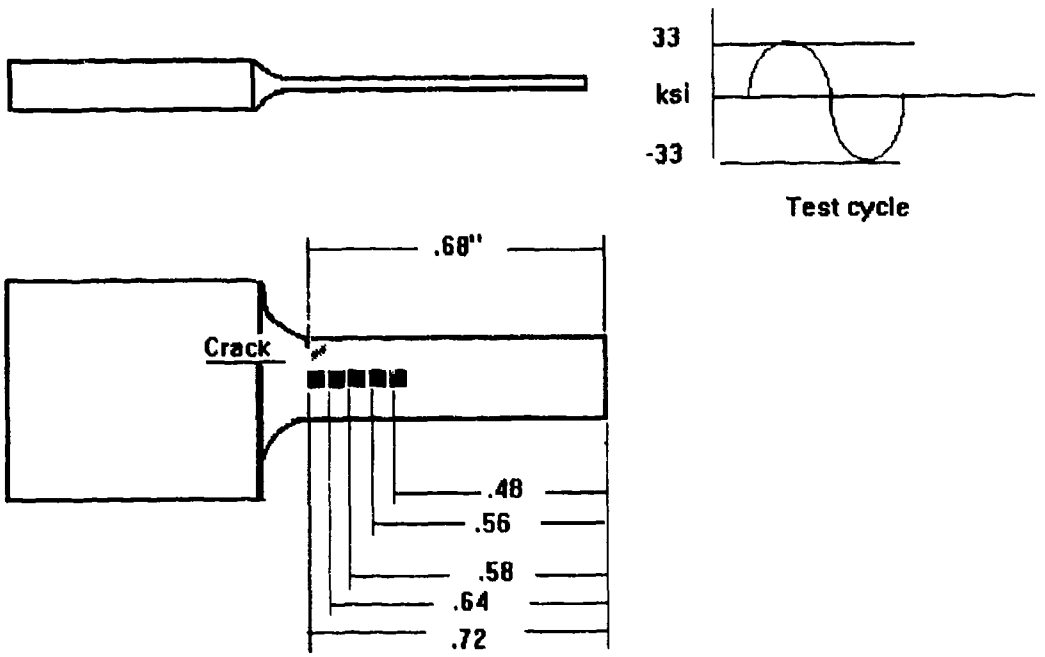

Figure 7: Schematic of test specimen and gage location on vibratory threshold test pecimen.

reaching 10^7 cycles (considered HCF runout) in a relatively short time permitting frequent inspection (via SEM). Test temperature was 78°F. The specimen gage section was metallographically prepared so IMQ defects in the high stress portion of the gage section (where sub critical growth from defects should occur) could be documented. A representative area is shown in Figure 8. The stress was incrementally increased following periodic inspections at 10^7 cycle intervals. The process was repeated until defects were seen to propagate. Following 10^7 cycles at 28 ksi with no growth, crack propagation was detected at $3x10^6$ cycles. Growth, from a .0029" micropore (Figure 9), totaled .092" at 33 ksi . Propagation, detected via a frequency drop, occurred abruptly over no more than $3x10^4$ cycles. The propagation mode was crystallographic (Figure 10) but the growth rate was too rapid to report sub critical crack propagation. The calculated stress intensity (K) for the defect, based on the runout stress of 28 ksi prior to propagation, was 4 ksi $\sqrt{in.}$. This sub-threshold stress intensity value is consistent with previous load shedding threshold determinations for PWA 1480 at room temperature prior to the plateau region where a fracture mode transition occurs. Extrapolation of the Region II behavior (microscopic transpercipitate (111) fracture) to near threshold growth rates is mechanistically correct since growth from the defect was transpercipitate (111) as in the load shedding test with the only difference being that the load shedding test exhibited microscopic rather than monoplanar (111) fracture.

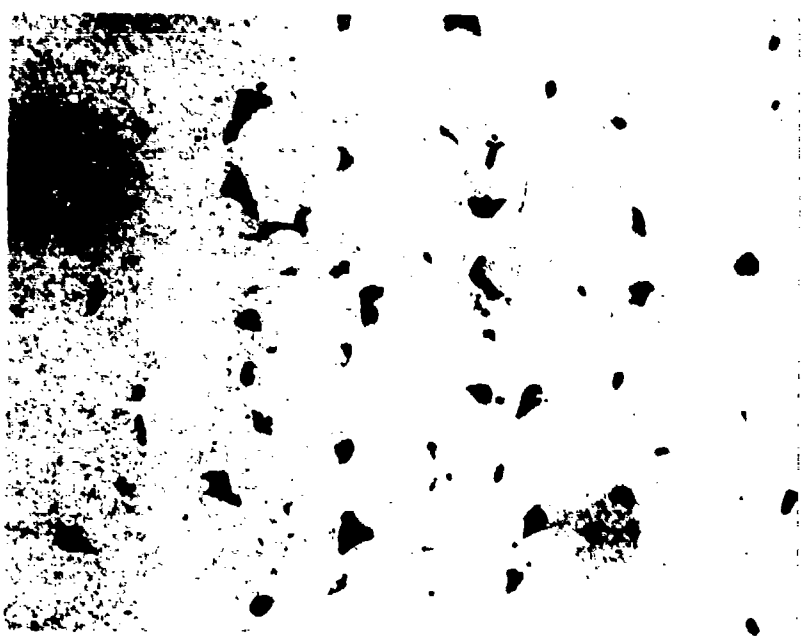

Figure 8: Typical area of mapped IMQ defects from max stress plane in vibratory test specimen (100X).

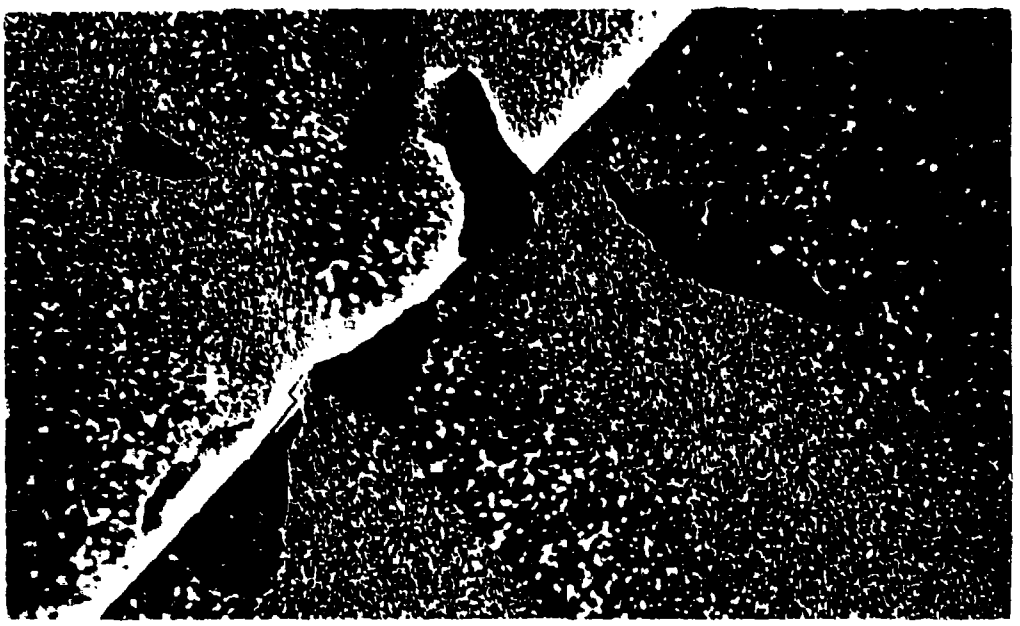

Figure 9: (111) crack initiation at two connected micropores. (630X).

Figure 10: (111) crystallographic growth (32X).

Crack Advance in Octahedral Fracture

Octahedral cracks also initiate sub surface, usually at some point source intrinsic material quality (IMQ) defect. Common IMQ defects in PWA 1480 and PWA 1484 are carbides, microporosity and eutectic γ-γ' (the distributions of occurance were reported in previous reports). The near surface crack shown in Figure 11 emanates from a carbide and is propagating along a (111) plane. The crack was observed by serial sectioning through a turbine blade attachment. The condition, octahedral initiation, has been assumed to be associated with bearing load induced shear stress resolving on favorably oriented (111) slip systems although Figures 1 and 2 suggest otherwise. Fracture morphology of internal (111) crack initiations from point source defects are shown in Figures 12 and 13. The defects are eutectic γ-γ' and TaC resp ectively. In both cases the hexagonal crack front is evidenced by arrest marks and, upon higher magnification, by slip lines resulting from the operative <110> slip directions intersecting the global (111) slip plane from beneath.

These fractures illustrate the mechanisms of planar (111) crack advance. A schematic representation of the crack advance process occurring in these cases is shown in Figure 14 as

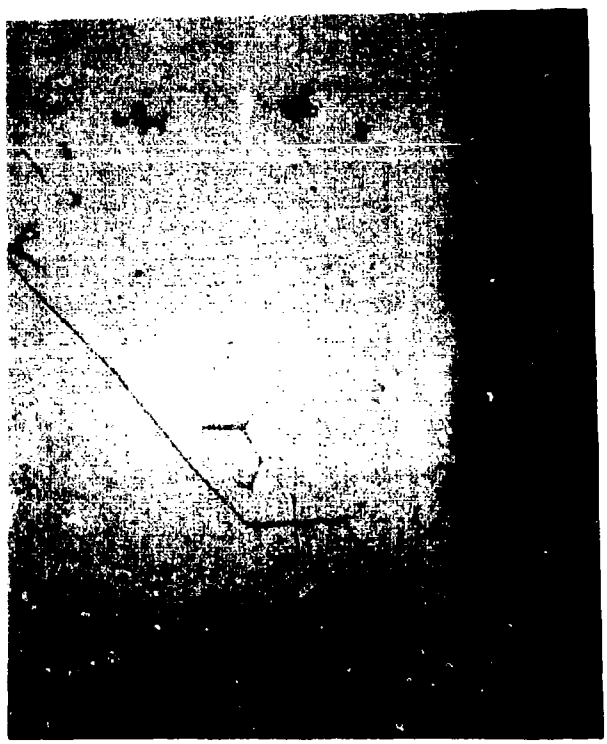

Figure 11: Cross section of sub surface (111) fatigue crack initiation at carbide in LPT blade root (320X).

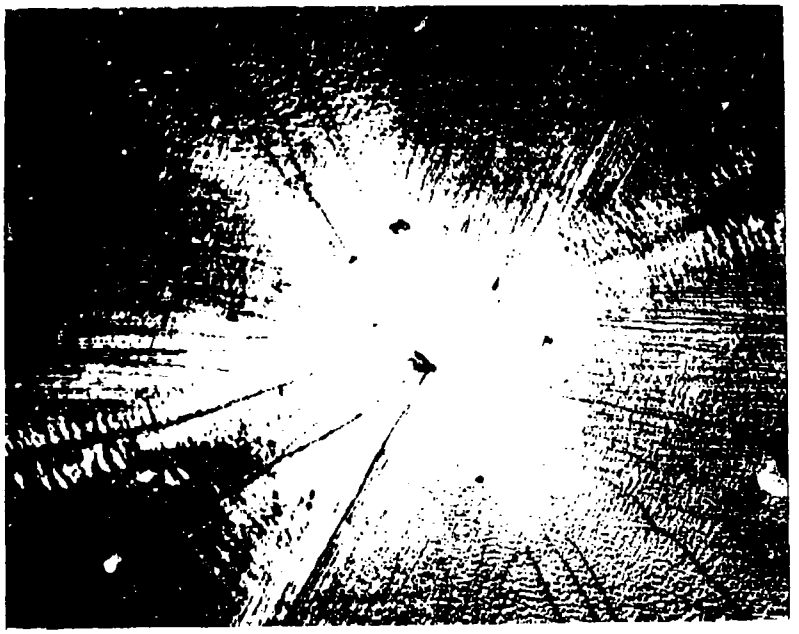

Figure 12: Fracture surface showing origin of sub surface (111) fatigue crack initiation (eutectic γ-γ') in PWA 1484 1100°F test specimen. Hexagonal crack front is an artifact of the operative slip systems (100X).

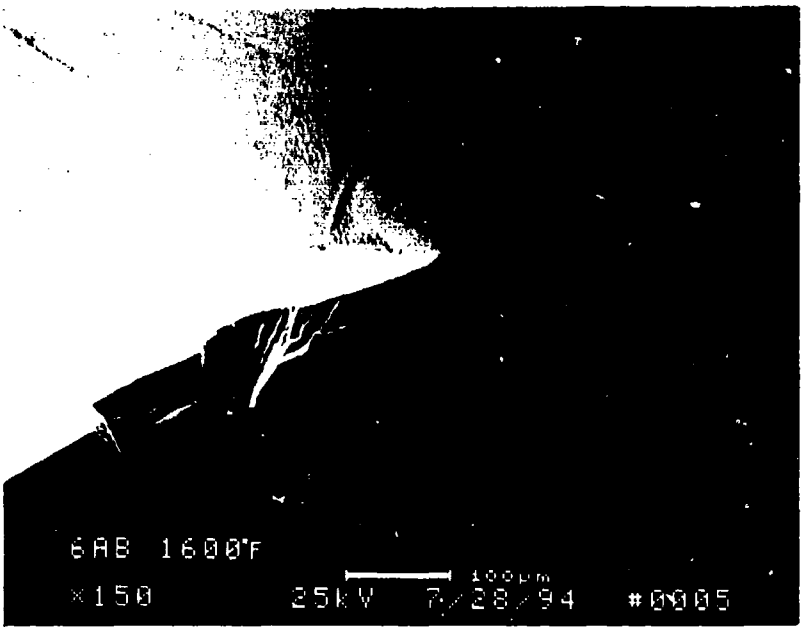

Figure 13: Mixed mode HCF crack initiation (internal origin at TaC) in PWA 1484 at 1600° F. Hexagonal crack front is an artifact of the operative slip systems.

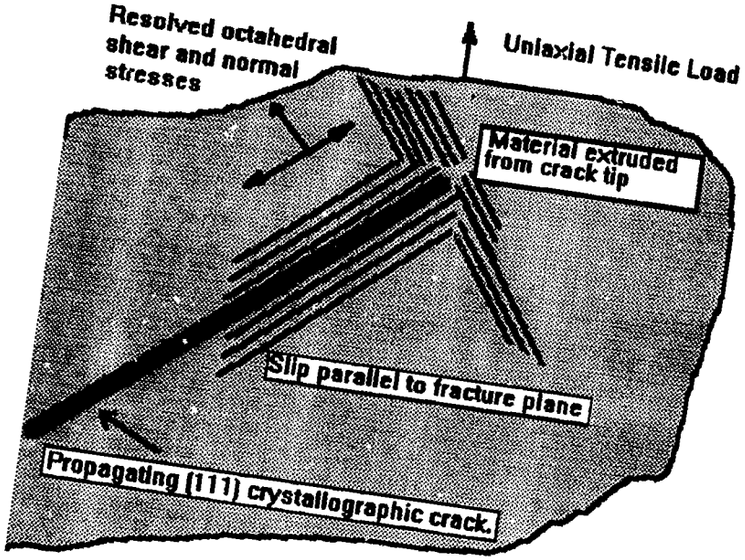

Figure 14: Schematic cross section through a propagating octahedral crack tip showing (111) slip parallel to the fracture plane. Intersecting slip planes ahead of crack tip. (theorized by Chen[1]) are transporting displaced material away from crack tip as crack advances.

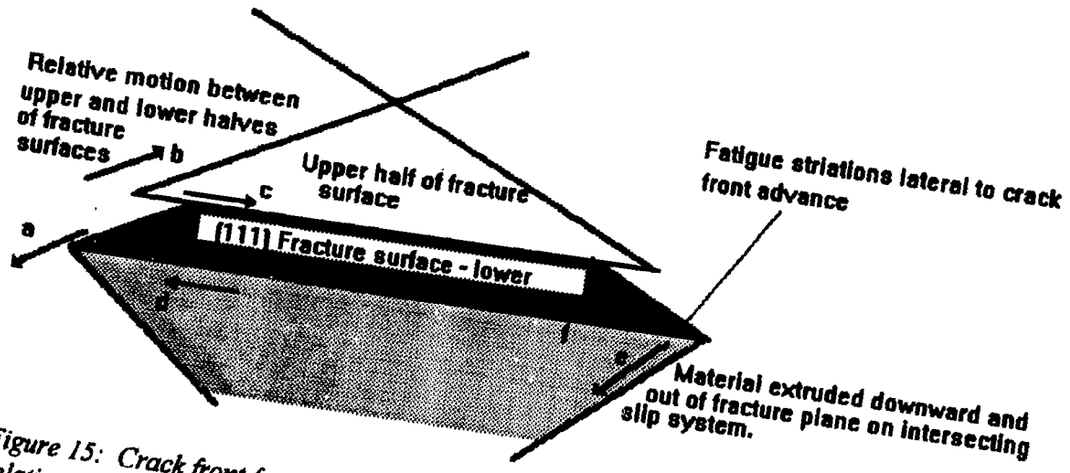

Figure 15: Crack front from the fracture in Appendix B, Figure 7. Arrows a and b show the relative motion between upper and lower fracture faces. <110> slip directions bound the triangular segment of the hexagonal plane of fracture. Arrows (d and e) show the lateral component of the a/b motion. Striations lateral to the advancing crack front are shown schematically at "f".

Figure 16: TEM of striations shown schematically at "f" in the previous figure (2800X).

a section through the propagating crack. Crack advance is accomplished as extruded material resulting from slip parallel to the (111) fracture planes is transported away from the crack tip by intersecting slip systems. Figure 15 is a head on view of the advancing crack in one of the hexagonal segments of the fracture shown in Figure 12. The relative motion between the upper and lower halves of the crack are indicated by the arrows at left (a and b) and are <110> slip directions that define the hexagonal segments of the fracture. The second set of arrows (d and e) show the resultant lateral component of the a/b motion. Fine striations lateral to the advancing crack front observed on the fracture are shown in Figure 16. Evidence of material transport by the intersecting slip system (e) is also present.

Energy Based Approach to Fracture

Energy based fracture life prediction is a subject of particular interest to P&W. The shearing of precipitates by dislocations that results in (111) fracture is resisted by atomic forces within the γ' superlattice, namely the antiphase boundary energy (APBE) and the superlattice intrinsic stacking fault energy (SISFE). These interfacial parameters are a function of superlattice chemistry. As binding energies they represent the resistive force in an energy balance equation where the driving force is the applied strain energy. The resultant microscopic fracture mode is the dependent variable in this equation and determines the fatigue crack growth rate. Understanding the relationships between crack growth rate, microscopic fracture modes, free surface energy and superlattice binding energies are necessary elements in moving toward an energy based fracture predictive system.

In an effort to better our understanding of binding energy and the effect on fracture matrix and superlattice, elemental profiles were obtained for PWA 1480 with a conventional precipitate morphology. Compositions were also obtained for γ and γ' in PWA 1480 with a modified microstructure. The results are shown in Table I and are plotted in Figures 17 and

Table I
Elemental composition of γ and γ' in PWA 1480 and Modified PWA 1480

LOC	PHASE	DIST (nM)	Al STD	Al MOD	Ti STD	Ti MOD	Cr STD	Cr MOD	Co STD	Co MOD	Ni STD	Ni MOD	Ta STD	Ta MOD	W STD	W MOD
8	Gamma	-48	0.81		0.28		29.43		12.83		52.31		0.49		3.83	
6	Gamma	-74	0.41		0.35		27.97		13.05		51.57		1.63		5.02	
7	Gamma	-14.5	0.71		0.53		26.27		12.02		54.99		1.5		3.99	
5	Prime	23	5.56		1.63		2.14		3.42		75.2		10.14		1.91	
4	Prime	159	3.86		2.1		2.18		3.72		76.17		10.71		1.26	
3	Prime	169	5.17		1.99		1.98		3.06		75.51		10.73		1.56	
2	Prime	182	4.75		1.88		2.19		3.05		76.17		10.38		1.59	
1	Prime	301	4.96		2.03		2.23		3.03		73.45		12.96		1.33	
A	Gamma	-65		1.24		0.34		28.71		10.27		53.67		1.68		4.09
B	Gamma	-32		1.24		0.28		29.38		10.15		54.21		0.83		3.92
C	Prime	32		5.61		1.83		2.09		3.63		73.93		11.61		1.29
D	Prime	65		5.59		1.96		1.86		3.34		74.51		11.43		1.31
E	Prime	129		5.19		1.89		2.25		3.44		74.52		11.95		0.75

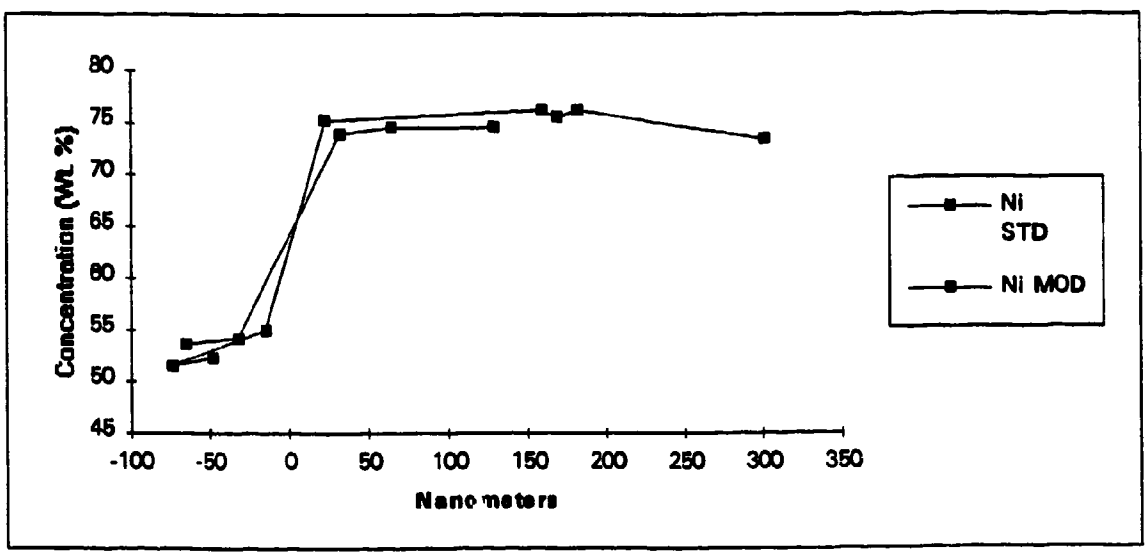

Figure 17: Distribution of Ni in γ and γ' for standard and modified PWA 1480. The γ/γ' interface is at zero nanometers.

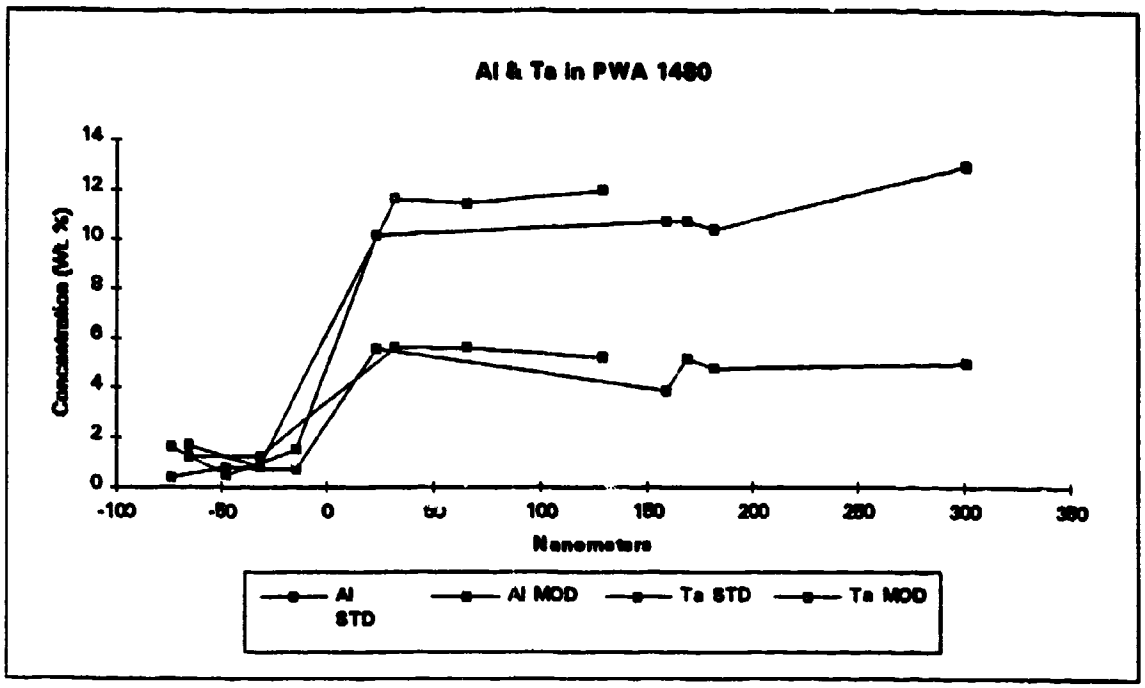

Figure 18: Distribution of Al and Ta in γ and γ' for standard and modified PWA 1480. The γ/γ' interface is at zero nanometers.

18 . The modified microstructure exhibits precipitate shearing under conditions where the conventional microstructure does not. This microscopic fracture mode transition is beneficial, producing a significant reduction in crack growth rate under certain conditions. The change is theorized to stem from a difference in γ' phase composition.

Planned Work

Modifications in superlattice chemistry will affect the γ' energy profile. As such, these chemistries will be considered for study via an atomistic simulation technique. The objective of this study will be to catalogue the energy profile for the γ' compositions for standard and modified PWA 1480. The difference in stress intensity (applied energy) for the fracture mode transition from matrix failure to precipitate shearing will be compared to the calculated binding energies. An understanding of the effects of superlattice chemistry on the K dependent microscopic fracture mode transition behavior in PWA 1480 is the end objective of this work.

References

1. O. Y . Chen: Ph.D. Dissertation, University of Connecticut, Stores, CT, 1985
2. G. R. Leverant and M. Gell, Met. Trans. A, 6A, 1975, p. 367

APPENDIX A

II. Program Organization

The program is structured into four tasks, three technical and one reporting. The individual tasks are outlined here.

Task 100 - Micromechanical Characterization

This task will define the mechanisms of damage accumulation for the various types of fracture observed in single crystal alloys. These fracture characteristics will be used to establish a series of Damage States which represent the fatigue damage process. The basis for this investigation will be detailed fractographic assessment of failed laboratory specimens generated in concurrent programs. Emphasis will be on specifically identifying the micromechanical damage mechanisms, relating them to a damage state, and determining the conditions required to transition to an alternate state.

Task 200 - Analytical Parameter Development

This task will extend current methods of fatigue and fracture mechanics analysis to account for microstructural complexities inherent in single crystal alloys. This will be accomplished through the development of flexible correlative parameters which can be used to evaluate the crack growth characteristics of a particular damage state. The proposed analyses will consider the finite element and the hybrid Surface-Integral and Finite Element (SAFE) methods to describe the micromechanics of crack propagation.

Task 300 - Probabilistic Modeling

This task will model the accumulation of fatigue damage in single crystal alloys as a Markov process. The probabilities of damage progressing between the damage states defined in Task 100 will be evaluated for input into the Markov model. The relationship between these transition probabilities and fatigue life will then be exploited to establish a model with comprehensive life predictive capabilities.

Task 400 - Reporting

Running concurrently with the analytical portions of the program, this task will inform the Navy Program Manager and Contracting Officer of the technical and fiscal status of the program through R&D status reports.

III. Technical Progress

We have repeatedly pointed out that global octahedral fracture plays a pivitol role in cataloging damage states in single crystal (SC) alloys. An understanding of the conditions under which this mode becomes operative and the effect it has on threshold and da/dN behavior is of critical importance to life prediction.

In previous monthly progress reports, we have described a hierarchy of microscopic fracture modes that exert a controlling influence on fatigue crack growth (FCG) behavior in PWA 1480 and PWA 1484. The effect these modes have on crack growth rate can be compared directly in constant cyclic stress intensity tests where some other parameter such as frequency or environment is varied to initiate a fracture mode transition. These fracture mode comparisons are facilitated by the fact that they can all be observed under Mode I loading conditions and analyzed with a Mode I stress intensity solution.

Global octahedral fracture can not be readily be compared to the others because it is driven by shear loading.

For global or monoplanar (111) fracture to occur in FCG testing a Mode II loading component is required. In Mode I testing unwanted (out of plane) crystallographic fracture frequently occurs on (111) planes that are not perpendicular to the direction of applied load. In this case, although octahedral fracture is produced, it can not be analyzed with a Mode I crack growth stress intensity solution. In tests where the (111) crystallographic plane is subjected to pure Mode I loading, fracture is non crystallographic, again preventing us from characterizing (111) fracture. This situation is described in Figure 1.

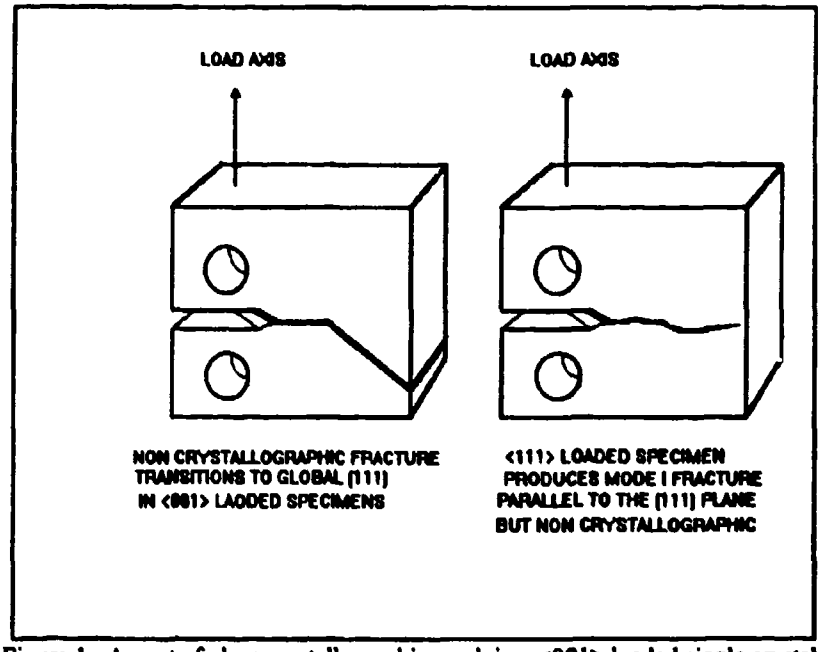

Figure 1. An out of plane crystallographic crack in a <001> loaded single crystal FCG specimen (Left). A <111> loaded specimen produces noncrystallographic fracture roughly parallel to (111) planes (Right).

Techniques for obtaining Mode II da/dN vs. ΔK data are available. Two methods are shown in figure 2. The beam specimen iis 4 point loaded to obtain shear at its center. In Figure 3 the "Brazilian Disk" specimen is compressivly loaded at its diameter. The angle of the starter notch with respect to the load direction is set to produce shear parallel to the preflaw.

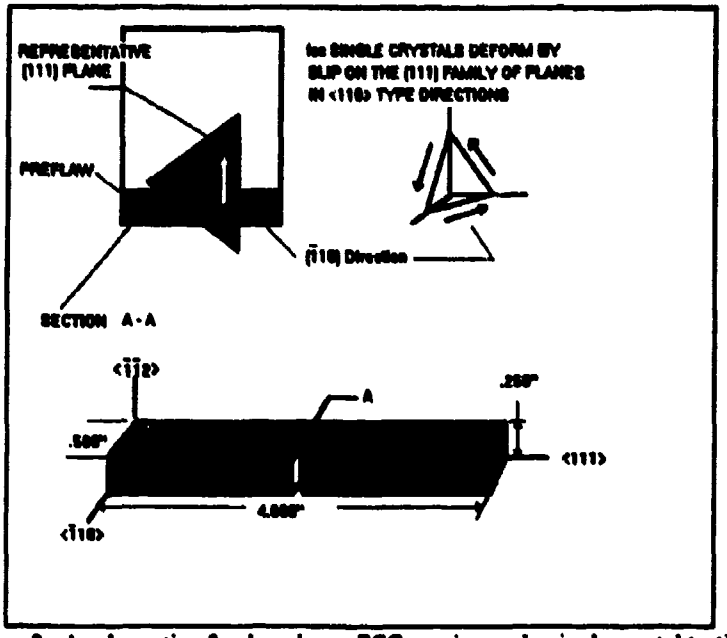

Figure 2. A schematic of a shear beam FCG specimen. In single crystal testing, the materials' preferred slip plane and direction are positioned coincident with the specimen shear plane.

In evaluating octahedral shear it is of critical importance that the material's shear plane, the (111) plane, be positioned (with extreme accuracy) coincident with the specimen's shear plane. In this way a comparison of crystallographic shear can be made with non crystallographic shear. Further, octahedral slip occurs on the (111) in specific directions (the <110> family of crystallographic directions). It may also be useful to study the effect of loading direction on crystallographic fracture by considering loading direction as a variable. This is shown schematically in Figures 4 and 5.

In work planned for the coming month we shall examine this fracture mode more closely.

IV. Current Problems

No technical problems have been encountered during the reporting period.

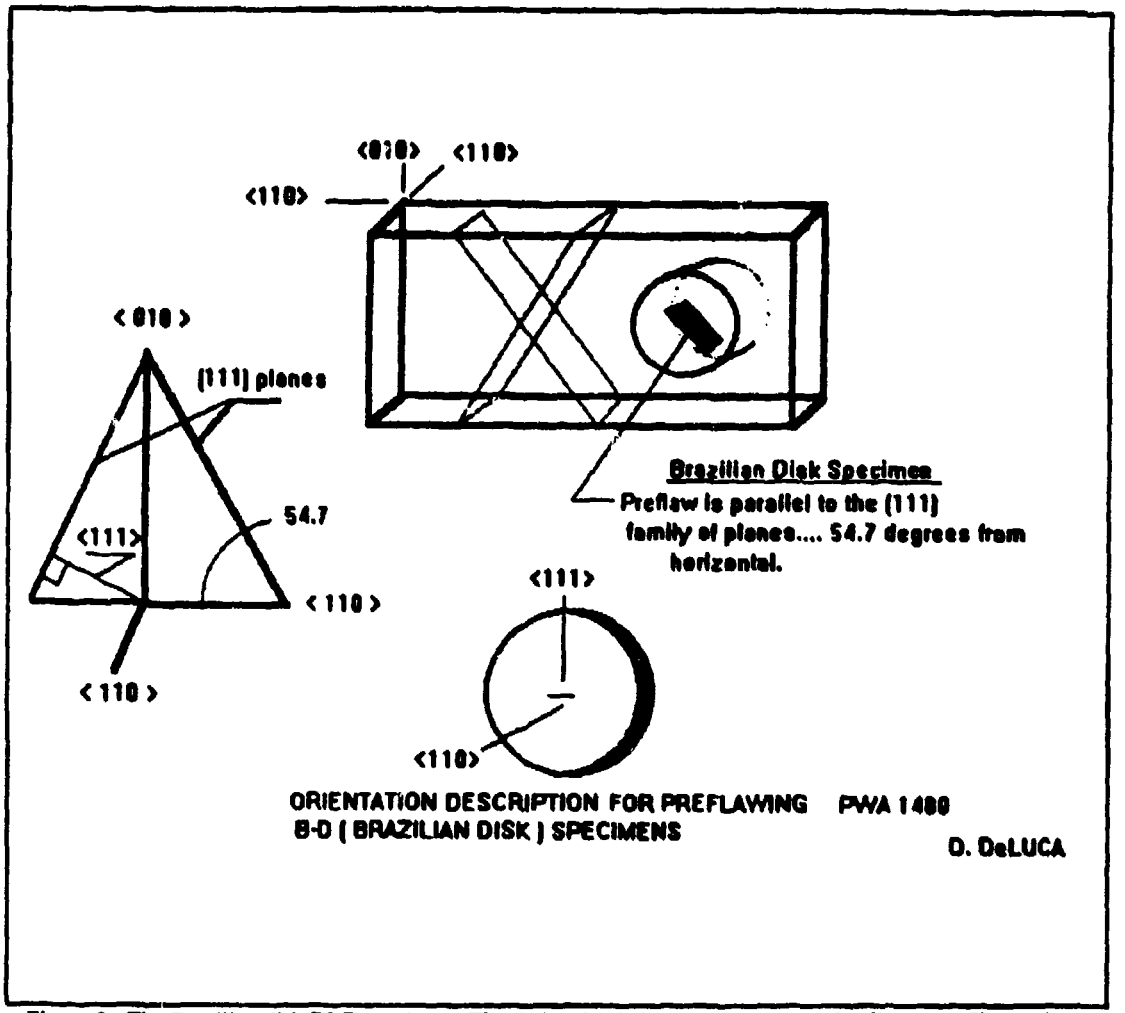

Figure 3. The Brazilian disk FCG specimen. The disk is loaded in compression at the diameter. The angle of the preflaw with the load axis determines the crack tip loading conditions. Obtaining properly oriented specimens is critical in evaluating (111) FCG data.

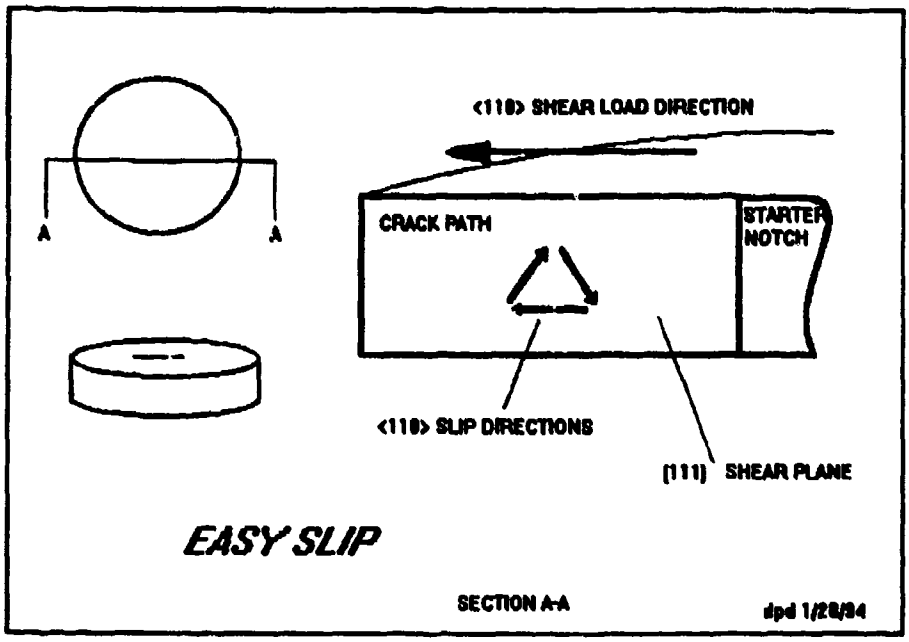

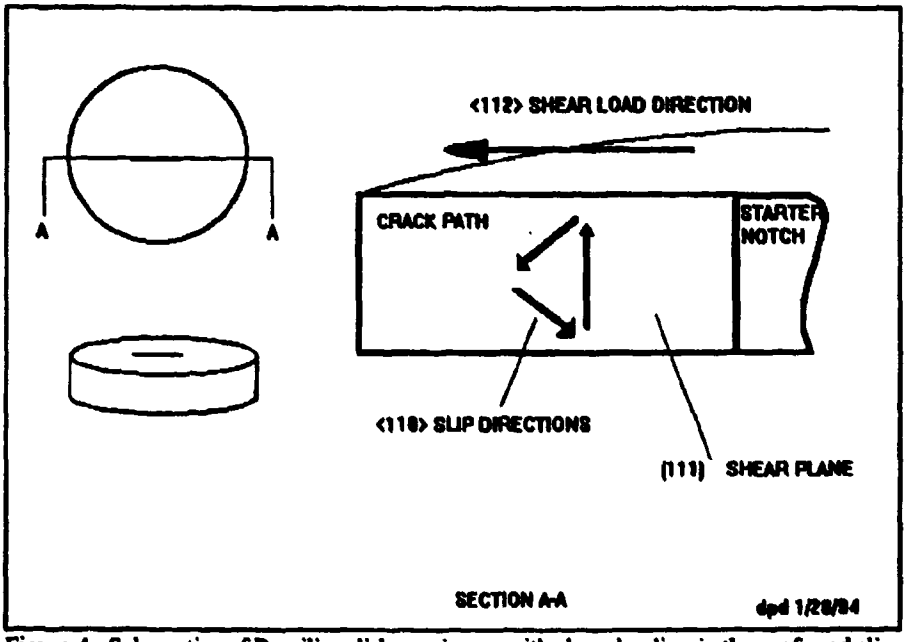

Figure 4. Schematics of Brazilian disk specimens with shear loading in the preferred slip direction (easy slip), at top, compared to shear loading oblique to the preferred slip direction, at bottom.

APPENDIX B

Markov model. The relationship between these transition probabilities and fatigue life will then be exploited to establish a model with comprehensive life predictive capabilities.

Task 400 - Reporting

Running concurrently with the analytical portions of the program, this task will inform the Navy Program Manager and Contracting Officer of the technical and fiscal status of the program through R&D status reports.

III. Technical Progress

We are currently examining the conditions that cause macroscopic (111) fracture to become operative and the various limits under which global (111) propagation becomes an available fracture mode. The fundamental elements of single crystal deformation provide a basis for understanding the cyclic behavior of PWA 1480 and PWA 1484.

Single crystals deform by shearing along (111) crystallographic planes, sometimes referred to as "octahedral" planes. This shearing occurs in the <110> family of directions (Figures 1- 2). The direction of load application with respect to crystal orientation determines the resolved shear stress for each of the (111)/<110> slip plane/direction sets constituting particular slip systems. As applied load is increased, additional slip systems become operative, making it possible for multiple slip systems to be operative simultaneously. An operative slip system is one where the resolved shear stress is sufficiently high to cause slip. This shear yield stress (τ_C) is also referred to as the materials critical resolved shear stress (CRSS). At a given applied load, more than one slip system may see resolved shear stresses in excess of τ_C (dependent upon orientation). Only the <123> orientation permits a single slip condition (only one slip system operative) to occur making it a useful orientation for study purposes.

The mechanisms of crystallographic fatigue crack initiation and fatigue crack propagation on a single macroscopic (111) plane are of critical importance to a mechanistically based life prediction system. An example of a "global" octahedral slip/initiation and the conditions which produced it are given in the following discussion.

If the applied stress is sufficiently low, (such that only one slip system is operative) a global slip plane can develop. This condition is shown in Figure 3, a photograph of a slip band observed in a smooth (K_t=1), <001> oriented PWA1480 high cycle fatigue (HCF) specimen tested at 20Hz, 26C, R=0.5, in high pressure hydrogen. The global slip band was observed on the surface after the specimen was retired at 10,000,000 cycles.

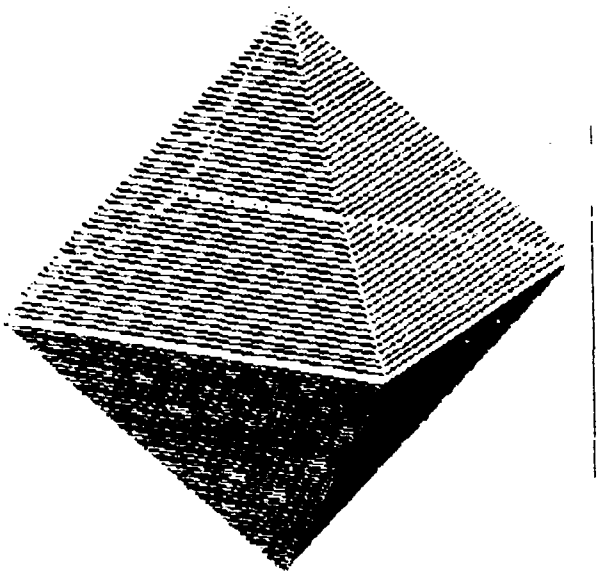

Figure 1. The octahedron described by eight (111) planes.

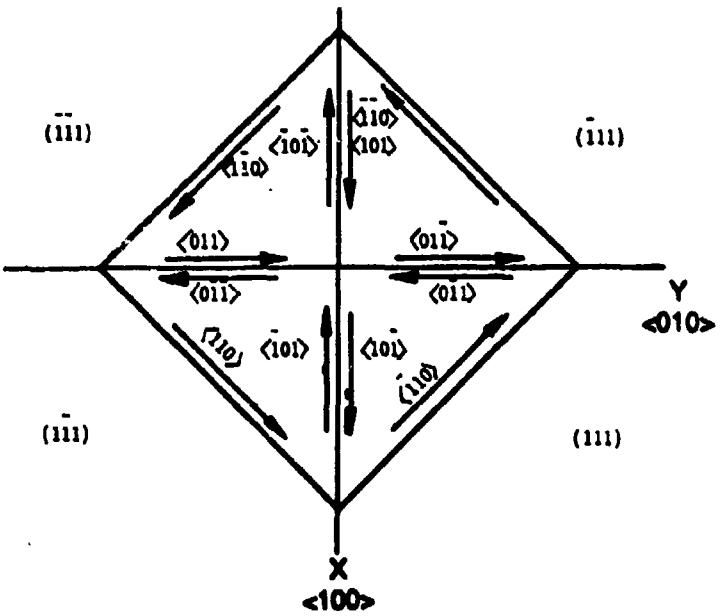

Figure 2. The octahedron viewed from the positive Z axis showing the 12 possible (111)/<110> slip systems.

Figure 3. A photograph of a slip band observed in a PWA 1480 HCF test specimen gage section. 5X

Global octahedral failure is the result of strain localization on a single slip system. The deformation preceding fracture is non-homogeneous, planar in nature, and occurs in localized intense or "persistent" slip bands. An example is shown in Figure 4.

Cyclic stressing produces alternating slip reversals that progress to slip band extrusion. Surface crack initiation occurs at these extrusion/intrusions aided in air as an oxidation mechanism precludes slip reversal. A single slip system is able to advance a crack under these circumstances. Our observations suggest that a critical slip displacement is reached before fracture can occur. A higher magnification view (Figure 5) of the specimen shown in Figure 3 reveals a 0.002" crack forming along the persistent slip band at the specimens surface.

Octahedral cracks also initiate sub surface, usually at some point source intrinsic material quality (IMQ) defect. Common IMQ defects in PWA 1480 and PWA 1484 (the subject of previous reports) are carbides, microporosity and eutectic $\gamma - \gamma'$.

The near surface crack shown in Figure 6 initiated at a carbide and is propagating along a (111) plane. The crack was observed by serial sectioning through a PWA 1422 turbine blade attachment test. The condition, octahedral initiation, is thought to be associated with bearing load induced shear stress resolving on favorably oriented (111) slip systems.

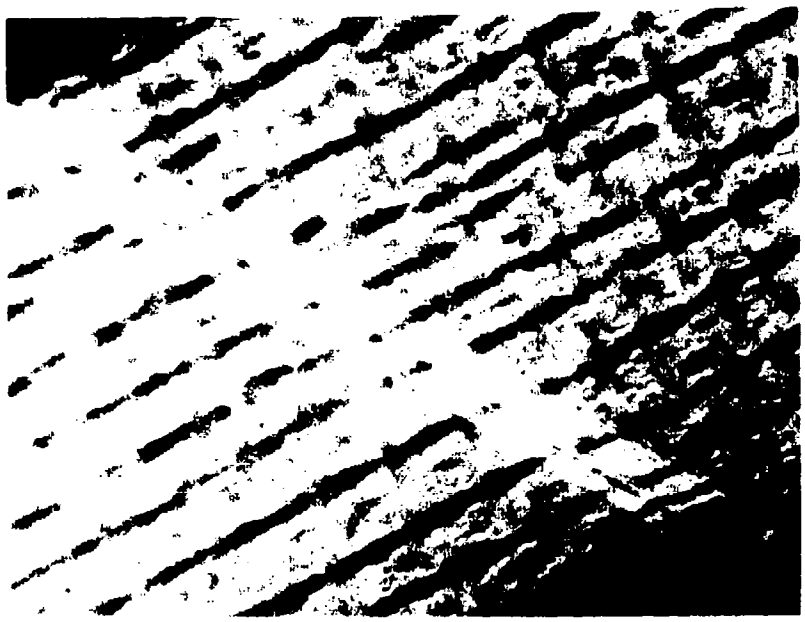

Figure 4: An intense or persistent slip band viewed metallographically and enhanced by polarized light (from Figure 3). Persistent slip bands evolve as initial precipitate shearing by dislocations compromises the order in the γ' superlattice. This creates preferential avenues for further dislocation penetration through the weakened superlattice. 40X

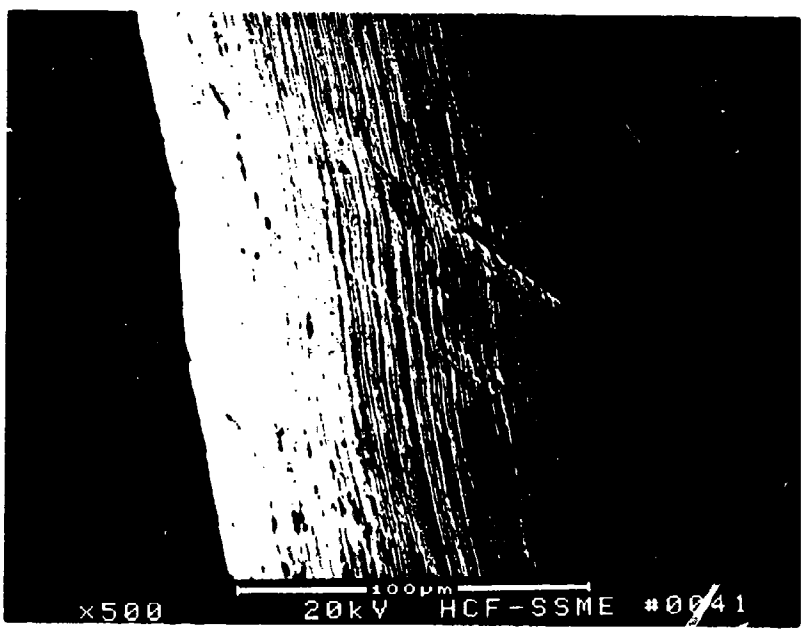

Figure 5. A 0.002" crack forming along a persistent slip band. The amount of slip displacement can be seen silhouetted at the specimen surface.

A second example of a subsurface octahedral fatigue crack is shown in Figure 7. The crack initiated at an IMQ defect (eutectic γ - γ') in PWA 1484 at 1100F, R=0.1, 136 ksi, 20Hz after 1360000 cycles and propagated in a vacuum.

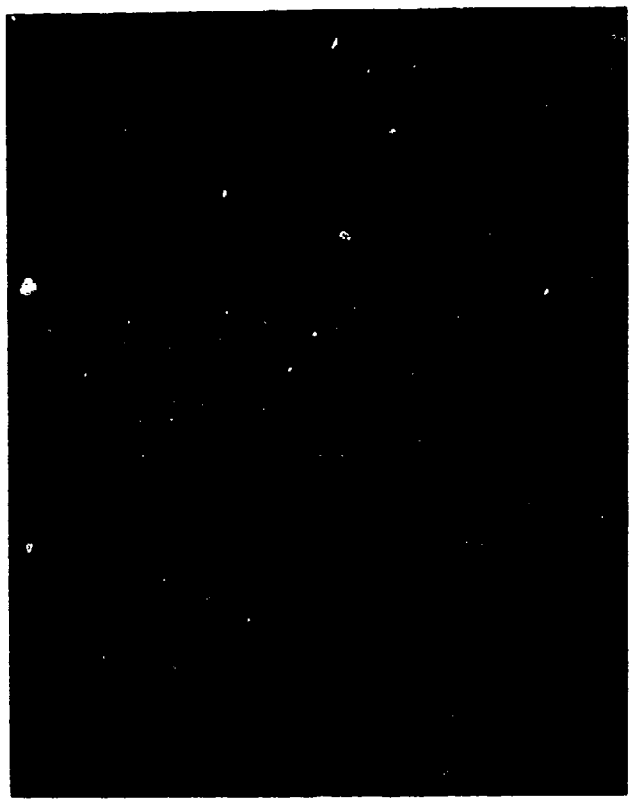

Figure 6. A subsurface fatigue crack initiating at a carbide in PWA 1422 and propagating along octahedral planes. 320X

Chen (1) concluded that in a vacuum, there is no clear distinction between crystallographic crack initiation and propagation processes. He suggests that initiation is by material displacement and transport by a cross-slip/extrusion mechanism requiring at least two operative slip systems to transport extruded material away from the crack tip. Slip occurs out of the fracture plane and lateral to the advancing crack front on intersecting slip systems (shown schematically in Figure 8).

A detailed study of the fracture shown in Figure 7 shows that multiple <110> family slip directions on the global (111) fracture plane are operative. Of particular interest is the presence of slip lateral to the direction of propagation

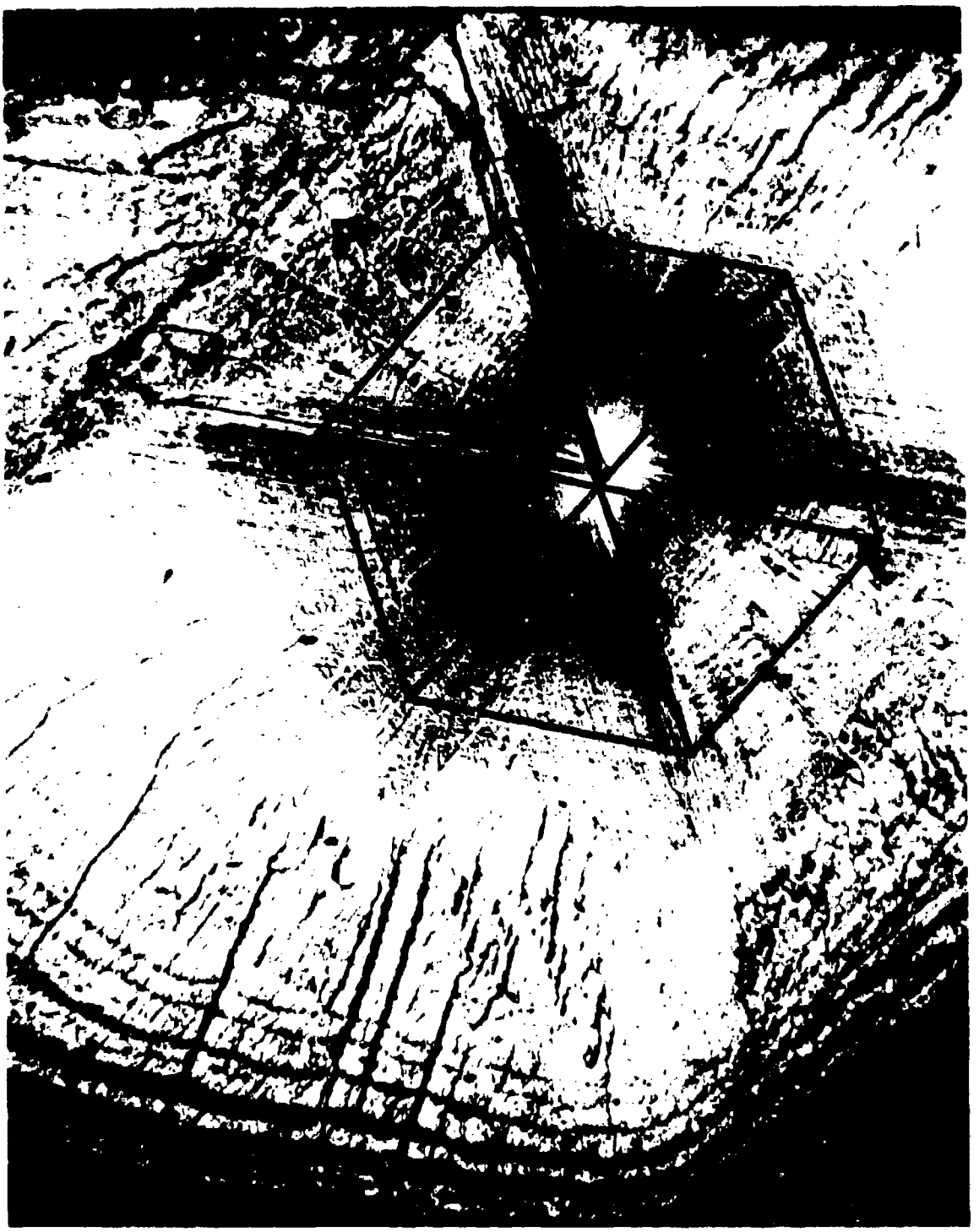

Figure 7. A (111) fracture surface in PWA 1484. The point source defect is eutectic γ - γ'. The hexagonal crack front results from three <110> slip directions being operative. The <110> directions are superimposed. (120X)

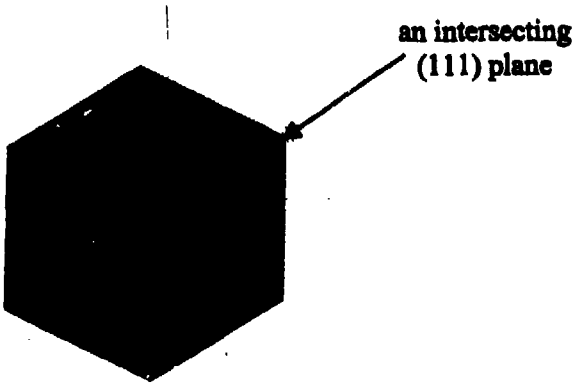

Figure 8. Fine secondary cracks parallel to the <110> slip directions visible in previous figure indicate cross slip on (111) planes (shown schematically) intersecting the fracture plane from beneath.

Figure 9. Cyclic lateral translation of material at the crack tip appears to be producing fine striations on the fracture surface lateral to the direction (112) of crack advance. (500X)

REPORT DOCUMENTATION PAGE	1. REPORT NO. FR21998-24	2.	3. Recipient's Accession No.
4. Title and Subtitle FATIGUE IN SINGLE CRYSTAL NICKEL SUPERALLOYS Technical Progress Report			5. Report Date 15 October, 1994 6.
7. Author(s) D. P. DeLuca and Charles Annis			8. Performing Organization Rept. No.
9. Performing Organization Name and Address United Technologies Pratt & Whitney P. O. Box 109600 West Palm Beach, FL 33410-9600			10. Project/Task/Work Unit No. 11. Contract(C) or Grant(G) No. (C) N00014-91-C-0124 (G)
12. Sponsoring Organization Name and Address Office of Naval Research Department of the Navy 800 N. Quincy Street Arlington, VA 22217-5000			13. Type of Report & Period Covered Technical 10/16/1993 - 10/15/1994 14.
15. Supplementary Notes			

16. Abstract (Limit: 200 words)

This program investigates the seemingly unusual behavior of single crystal airfoil materials. The fatigue initiation processes in single crystal (SC) materials are significantly more complicated and involved than fatigue initiation and subsequent behavior of a (single) macrocrack in conventional, isotropic, materials. To understand these differences is the major goal of this project.

17. Document Analysis a. Descriptors

Fatigue, Fracture, Single Crystan, PWA 1480, PWA 1484

b. Identifiers/Open-Ended Terms

c. COSATI Field/Group

18. Availability Statement	19. Security Class (This Report)	21. No. of Pages
Unlimited	Unclassified	31
	20. Security Class (This Page)	22. Price

(See ANSI-Z39.18) See Instructions on Reverse OPTIONAL FORM 272 (4-77)

* GPO : 1993 0 - 381-526 (8393)